

Changes in intense tropical cyclone activity for the western North Pacific during the last decades derived from a regional climate model simulation

Monika Barcikowska¹ · Frauke Feser² · Wei Zhang³ · Wei Mei^{4,5}

Received: 2 June 2015 / Accepted: 17 October 2016 / Published online: 29 March 2017
© The Author(s) 2017. This article is an open access publication

Abstract An atmospheric regional climate model (CCLM) was employed to dynamically downscale atmospheric reanalyses (NCEP/NCAR 1, ERA 40) over the western North Pacific and South East Asia. This approach is used for the first time to reconstruct a tropical cyclone climatology, which extends beyond the satellite era and serves as an alternative data set for inhomogeneous observation-derived records (Best Track Data sets). The simulated TC climatology skillfully reproduces observations of the recent decades (1978–2010), including spatial patterns, frequency, lifetime, trends, variability on interannual and decadal time scales and their association with the large-scale circulation patterns. These skills, facilitated here with the spectral nudging method, seem to be a prerequisite to understand the factors determining spatio-temporal variability of TC activity over the western North Pacific. Long-term trends (1948–2011 and 1959–2001) in both simulations show a strong increase of intense tropical cyclone activity. This

contrasts with pronounced multidecadal variations found in observations. The discrepancy may partly originate from temporal inhomogeneities in atmospheric reanalyses and Best Track Data, which affect both the model-based and observational-based trends. An adjustment, which removes the simulated upward trend, reduces the apparent discrepancy. Ultimately, our observational and modeling analysis suggests an important contribution of multi-decadal fluctuations in the TC activity during the last six decades. Nevertheless, due to the uncertainties associated with the inconsistencies and quality changes of those data sets, we call for special caution when reconstructing long-term TC statistics either from atmospheric reanalyses or Best Track Data.

Keywords Tropical cyclones · Typhoons · Regional downscaling · North Western Pacific · Climate change · Climate variability · Multi-channel singular spectrum analysis

Electronic supplementary material The online version of this article (doi:10.1007/s00382-016-3420-0) contains supplementary material, which is available to authorized users.

✉ Monika Barcikowska
monikabarcikowska@noaa.gov; mbarcikowska@edf.org

¹ Princeton University, GFDL Princeton University Forrestal Campus, 201, Forrestal Road, Princeton, NJ 08542, USA

² Helmholtz-Zentrum Geesthacht Centre for Materials and Coastal Research, 21502 Geesthacht, Germany

³ IIHR - Hydroscience and Engineering, University of Iowa, Iowa City, IA, USA

⁴ Scripps Institution of Oceanography, University of California at San Diego, La Jolla, CA, USA

⁵ Department of Marine Sciences, University of North Carolina at Chapel Hill, Chapel Hill, NC, USA

1 Introduction

Tropical cyclone (TC) activity over the last five decades has recently gained substantial attention, leading to a debate on global warming and its potential impact on TC variability. Unfortunately, in the western North Pacific basin (WNP) TC statistics derived from different observation-derived data sets ('Best Track Data', hereafter referred to as BTD) show strong discrepancies. These differences imply severe inhomogeneities (Barcikowska et al. 2012; Ren et al. 2011; Kamahori et al. 2006; Wu et al. 2006), impacting mostly the highest TC intensity records. Therefore results based on BTD relating to TC variability and changes due to global warming/increasing sea surface temperature (SST) are inconclusive and questionable.

Atmospheric reanalyses are an alternative source of data, potentially useful for deriving storm statistics, given sufficiently long and homogenized observational data sets. However, the coarse spatial resolution of reanalyses limits the possibility of deriving realistic features of meso-scale phenomena like TCs. General circulation models (GCMs) or atmospheric general circulation models (AGCMs) with relatively high horizontal resolution (up to 20 km horizontal resolution) were used recently for future climate projections (Knutson et al. 1998; Bengtsson et al. 2007; Camargo and Barnston 2009; Oouchi et al. 2006; Vitart et al. 1997; Kamahori et al. 2011; Murakami et al. 2012). However, these studies are still not providing univocal results. Large parts of the studies indicate a decrease in TC frequency, but also an increase in more intense TCs (Sugi et al. 2002; Sugi and Yoshimura 2004, 2012; Knutson et al. 1998; Bengtsson et al. 2007; Zhao et al. 2007). However, Stowasser et al. 2007 projected an increase of TC frequency. Mei et al. (2015) reconstructed a TC climatology over the WNP for the last three decades, using the Geophysical Fluid Dynamics Laboratory (GFDL) High-Resolution Atmospheric Model (HiRAM, 25-km horizontal resolution) forced with observed SST. Authors found a strong decadal signal, associated with the SST changes in the tropical Central Pacific. However, a relatively high interannual variability of TCs, compared to the length of the simulations (1978–2008), constrained feasibility of extracting statistically meaningful signals of TC variations.

Large uncertainty of the derived results stems from the biases in simulated large-scale environmental conditions and these can be associated with the model's relatively low skill in simulating interannual or decadal-scale variability of TC activity. Nevertheless, some studies (e.g. Iizuka and Matsuura 2008; Zhang et al. 2016) demonstrated that a coupled ocean–atmosphere general circulation model (CGCM), can skillfully capture a relationship between WNP TC activity and ENSO. The statistical/downscaling method of Emanuel et al. 2008 allowed to reproduce with reasonable skill the observed variability of TCs power dissipation.

The dynamical downscaling approach provides an opportunity to reconstruct a long-term and homogeneous TC climatology with significantly reduced computational costs. A number of studies demonstrated high skill of atmospheric regional climate models (RCMs) to downscale meso-scale features of TCs (Feser and von Storch 2008a, b; Walsh et al. 2004; Knutson et al. 2007; Wu et al. 2014; Au-Yeung and Chan 2012; Huang and Chan 2014). Although simulated TC intensities are often too small compared to observed values, they are still more realistic than those in global reanalyses. Knutson et al. (2007) showed that

dynamical downscaling of NCEP atmospheric reanalyses with an 18-km grid RCM utilizing spectral nudging, successfully reproduces the observed interannual TC variability over the North Atlantic basin between 1980 and 2006.

Wu et al. (2014) followed the approach of Knutson 2007 for the western North Pacific. But the authors were not able to reproduce the interannual variability of TC activity, mostly due to a weak/absent relationship with ENSO (Camargo et al. 2007; Wang and Chan 2002). Wu et al. (2012) examined the internal variability in downscaling simulations of the WNP climate, and reduced its impact by using an average over ensemble simulations.

A detailed analysis of TC activity over the WNP and determination of their interannual and decadal-scale variations is important. It could help to understand the impact of future changes in large-scale circulation on TC activity and therefore enhance a potential skill for TC activity predictions. Due to the high computational costs of high-resolution regional climate simulations (even though smaller than for high-resolution GCM simulations), these models have not yet been applied to hindcast TC climate for more than three decades.

This study investigates a present-climate typhoon climatology, reconstructed using an atmospheric RCM. Two simulations are performed, for the periods 1948–2011 and 1959–2001. These are the first such long-term regional hindcast simulations focusing on typhoons. The climatology is derived with a regional atmospheric model, driven by two coarsely resolved atmospheric reanalyses, provided by NCEP/NCAR [National Center for Environmental Prediction/National Center for Atmospheric Research, (Kalnay et al. 1996)] and by the European Centre for Medium-Range Weather Forecast (ERA-40, Uppala et al. 2005). Using such a temporally stationary model system can potentially lead to more homogeneous typhoon climatologies than those derived from observational data sets. A shortcoming of this approach is that the quality of the derived results strongly depends on the quality of the atmospheric fields, which drive the RCM simulation. The potential inhomogeneities present in the reanalyses can be inherited by the model simulation.

The structure of the study is as follows: Sect. 2 describes the model settings, the statistical methods applied in the study, and the data. In the first part of Sect. 3, spatial features as well as intensity of downscaled TCs are compared with the observations (BTD). The second part of Sect. 3 focuses on temporal variations of the derived TC climatology. The third part analyzes the relationship between large-scale environmental patterns and interannual-to-decadal TC variability. The last part of Sect. 3 examines the differences in simulated TC intensity between the two reconstructions, which are based on different reanalyses. It also discusses

the uncertainty of the results, associated with the potential temporal inhomogeneities in the atmospheric reanalyses. Section 4 provides an interpretation for the results and summarizes the main findings.

2 Model, data and methodology

2.1 Model set up and global forcing data

The regional model applied in this study is the Cosmo-CLM (CCLM, www.clm-community.eu; (Rockel et al. 2008; Steppler et al. 2003), the climate version of the Lokal Modell of the German Weather service (Böhm et al. 2006). The NCEP/NCAR 1 reanalysis (Kalnay et al. 1996) (6-hourly resolution and a grid spacing of T62, 210 km) and the ERA-40 reanalysis (Uppala et al. 2005) (6-hourly resolution and a grid spacing of T159, 125 km) serve as initial conditions and forcing fields. The model was run in climate mode, which means that it was initialized with reanalysis data only at the very beginning and then run continuously for several decades, using the reanalysis data as boundary conditions. Additionally, CCLM was forced to follow the global state more closely, using a spectral nudging technique (von Storch et al. 2000). The technique was applied here only for horizontal wind components. It was shown by Feser and Barcikowska (2012) that spectral nudging is very efficient at reducing the RCM's internal variability. Consequently, the simulated large-scale climate was in very good agreement with the driving fields, and the representation of TC climatology significantly improved. The RCM wind fields were spectrally nudged within the entire model interior, starting at 850 hPa with increasing strength for higher model layers. Below 850 hPa, where regional-scale features are important, the RCM was not nudged. Sea surface temperature is provided by each of the reanalyses. The simulation area covers the region of the western North Pacific and South-East Asia within the region: 20°S, 110°E; 20°S, 180°E; and 45°N, 80°E; 45°N, 160°W. The grid spacing chosen for the model is 0.5° which amounts to about 55 × 55 km. The RCM was driven in the non-hydrostatic mode, using the standard parameterization and the Tiedtke (1989) convection scheme. For detailed model settings we refer the reader to Feser and von Storch (2008a, b).

2.2 Tropical cyclone detection and tracking algorithm

Hindcasted TC tracks were extracted with a tracking algorithm (Feser and von Storch 2008a, b) that searches for local minimum sea level pressure and maximum wind speed. Before tracking, a spatial digital band-pass filter (Feser and von Storch 2005) was applied to the 1-hourly output of sea level pressure fields to extract only meso-scale features like

TCs. A TC was identified when a wind speed maximum of 17.5 m s⁻¹ was reached, a pressure minimum of 995 hPa, a filtered pressure anomaly of -9 hPa and for duration times of more than 48 h. With these criteria the mean annual TCs number is comparable to observation-derived ones (BTD). In this case 1980–2007 was taken as a reference period. By then satellite observations were available, allowing for better homogeneity in observed TC records (Velden et al. 2006).

To identify TCs of categories 2–5 on the Saffir–Simpson Hurricane-Scale (hereafter referred to as intense TCs) the cyclonic system had to satisfy higher intensity criteria. However, intensity is often underestimated in 50-km horizontal resolution RCMs. Therefore, those criteria were calibrated subjectively to the frequency of the observed intense TCs, namely corresponding to the category 2–5 of the Saffir Simpson classification. This approach prevents from underrepresentation of the intense TCs frequency, which occurred in the previous studies (Knutson et al. 2007; Wu et al. 2014), extracting intense storms based only on their wind and pressure intensity.

2.3 Data and statistical methods

For comparison purposes we use BTD provided by the Japanese Meteorological Agency (JMA, www.jma.go.jp/jma/jma-eng/jma-center/rsmc-hp-pub-eg/besttrack.html), the China Meteorological Administration (CMA, <http://www.typhoon.gov.cn>), and the Joint Typhoon Warning Center (JTWC, www.usno.navy.mil). Access to all mentioned data sets were facilitated by the International Best Track Archive for Climate Stewardship (hereafter referred to IBTrACS; <http://www.ncdc.noaa.gov/oa/ibtracs/index.php?name=ibtracs-data>). Those data sets differ from one another, especially for TC intensities. Remarkable discrepancies are associated with inhomogeneities, caused by changing operational methods and observational sources and also lack of in situ measurements suitable for data validation (Barcikowska et al. 2012; Landsea et al. 2006). JMA BTD were found to be most useful in terms of temporal homogeneity and long-term statistics (Barcikowska et al. 2012). Remote sensing remarkably improved spatial homogeneity of TC measurements. Therefore measurements recorded since begin of the satellite era (1978) were used for comparison of the observation-derived and simulated spatial patterns of TC tracks. Previous studies (Barcikowska et al. 2012; Kamahori et al. 2006) indicated that TC climate statistics derived from independent BTD sets can be more univocal when analysis focuses collectively on TCs of intensity categories 2–5 of the Saffir–Simpson Hurricane Scale (hereafter referred to as intense TCs). Therefore the present study will pay particular attention to the statistics of the intense TCs.

For an analysis of the reanalysed decadal ocean–atmosphere variability over the Pacific we used annual sea surface temperature (SST) and monthly pressure at mean sea level (SLP), zonal wind and precipitation datasets are provided by NOAA-CIRES 20th Century Reanalysis V2c (20CR, Compo et al. 2011, http://www.esrl.noaa.gov/psd/data/-20thC_Rean/). All variables were further interpolated to a common $10^\circ \times 10^\circ$ lat-lon grid.

Simulated TC climatology was analyzed using metrics of seasonally (JASON) aggregated, basin-wide frequency for TCs (all intensity categories), intense TCs (falling into category 2–5 of Saffir–Simpson classification) and accumulated number of days for the intense TCs (i.e. intense TCs lifetime). The period of TC days analysis for CCLM driven by NCEP (hereafter referred to as CCLM-NCEP) is 1948–2011, 1959–2001 for CCLM driven by ERA-40 (hereafter referred to as CCLM-ERA), and 1951–2011 in BTD. For one BTD (JMA) statistics could be derived only since 1977, due to the lack of intensity recordings for the earlier period.

Seasonal fields of spatial density (SPD) of 6-hourly TC occurrences (SPD) were derived with the horizontal resolution of $5^\circ \times 5^\circ$ and for the period 1978–2001, when all data sets were available. Linear trend fields were derived from SPD fields, using least squares fit algorithm. Composite analysis of differences in the spatial TC density anomalies during the positive and negative ENSO phase was done based on values higher and lower than the 50th percentile of the NINO3.4 index in 1978–2010. This allowed us to use samples of 30 values falling into either ENSO positive or ENSO negative category. Analysis was repeated for the upper and lower 33th percentiles, which did not alter substantially the results. The NINO3.4 time series were downloaded from: http://www.esrl.noaa.gov/psd/gcos_wgsp/Timeseries/Nino34/.

The metrics used to analyze seasonal TC intensity are: mean TC intensity (m s^{-1}), and mean power dissipation index ($\text{m}^3 \text{s}^{-3}$) (hereafter referred to as mean PDI, Emanuel (2005, 2007)). Mean TC intensity at a certain location is derived by averaging seasonal accumulated maximum velocities of all passing TCs. For those calculations values of wind speed at each 6-hourly TC position were used.

An empirical orthogonal function (EOF) analysis was applied in order to define dominant spatial modes of simulated and BTD seasonal TC variability. Resulting ‘key’ patterns are derived from the anomalies of annual SPD fields for both CCLM simulations in the common period 1978–2001. The patterns, which explain a greater percentage of the variance in the input data are considered to be more dominant. An EOF analysis was also used to describe uncertainties of TC activity in CCLM reconstructions. The analysis was applied separately and jointly to annual fields of the differences between CCLM simulations (CCLM

NCEP minus CCLM ERA), for atmospheric temperature at 100 hPa, mean PDI, accumulated TC intensity (hereafter w_{max}) and accumulated TC occurrences (spd).

Analysis of decadal-scale variations of TC activity was done with Singular Spectrum Analysis (SSA). It is a non-parametric, data-adaptive method, which has been well described by Broomhead and King (1986), Fraedrich (1986), or Allen and Smith (1996).

The relationship between temporal TC variability and large-scale environmental conditions was analyzed with Multi-Channel Singular Spectrum Analysis (MSSA, Allen and Robertson 1996). MCSSA is an extended version of the SSA. It searches for spatially coherent temporal patterns. Therefore, assuming that dynamical mechanisms are time-scale selective, this method is more likely to extract signals representing single, dynamically meaningful mechanisms. As an eigenvalue-based method, MSSA decomposition is based on diagonalizing a matrix. The matrix is created with vector time series and embedded lagged-time series. Because the length of the time series is short, compared to the number of spatial channels (grid boxes), dimension of the dataset was primarily reduced to the first 10 leading PCA components (explaining more than 80% of variance). The lag window applied to the annual SST fields and TC time series is 20 years and the time interval is one year. This was done to enable extraction of statistically significant signals with temporal variability on a yearly-to-decadal time scale.

MSSA was repeated for the reanalysed annual 20CR SST and SLP dataset, for the larger domain and longer period. We used data for the Pacific region between 60°S and 60°N , spanning back to the early 20th century. Data was further reduced to the first leading 20 PCA components, analyzed with a lag window of 35 years. Sensitivity of the results was tested with the M lag window for $20 < M < 35$, which did not indicate substantial impact on the results. Significance of decadal-scale variability was tested using a Chi squared test.

Linear regression analysis was performed for annual values of 20CR SLP and zonal wind and precipitation, with significance tested with a F-statistic test for the analysis of variance.

3 Results

3.1 Simulated and observed TC climatology over the western North Pacific: spatial distribution and intensity

In this section, spatial and temporal features of TC occurrences reconstructed with CCLM are compared with BTD. The analysis focuses on interannual, decadal and climatological time-scale variability of TCs in the JASON

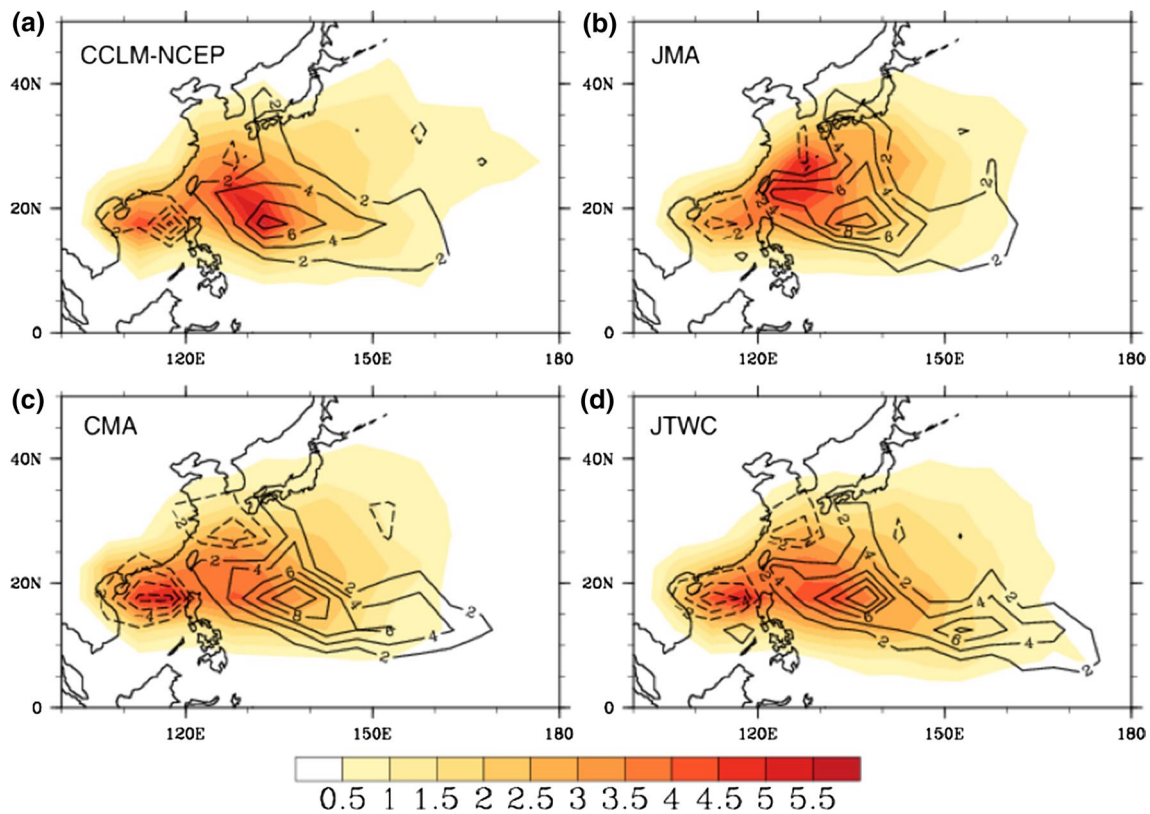


Fig. 1 Density (*shaded*) of the seasonal (JASON) 6-h TC occurrences, normalized by their spatial mean in **a** CCLM-NCEP simulation and BTD **b** JMA, **c** CMA, **d** JTWC, for the common period: 1978–2001. Numbers are shown for $5^\circ \times 5^\circ$ lat-lon boxes. Contours

show the composite difference in the yearly TC occurrences during the positive and negative ENSO phase (ENSO positive—ENSO negative). Contours with negative values are *dashed*

seasons of 1978–2010. BTD sets in this period are more reliable, since their primary observational sources are satellite-based measurements.

CCLM TC climatologies were extracted with a tracking algorithm set up to match the BTD mean annual TC frequency (26 TCs). The seasonal distribution of extracted TCs is slightly biased toward the cold season. Therefore seasonal (JASON) mean of CCLM-NCEP and CCLM-ERA simulations is slightly lower (17.3 and 17.9 TCs), than observations. BTD indicate 20.5, 22.6, 22.2 TCs for JMA, CMA, JTWC respectively. The standard deviations of these time series, shown in Fig. 4a, are comparable and reach values of 4.4 TC for CCLM-NCEP and 3.6/4.2/4. TC for JMA, CMA and JTWC respectively.

The hindcasted climatology of the spatial distribution shows very realistic features, and bears a close resemblance to the BTD. Figure 1 shows spatial densities, derived from hindcasted (CCLM-NCEP) and BTD TCs' 6-hourly trajectories between 1978 and 2001. The density fields are normalized by the mean spatial density; therefore they represent a directly comparable measure of TC concentration for all four data sets.

Both simulations (CCLM-NCEP, CCLM-ERA) skillfully reproduced the BTD patterns (CMA, JMA, JTWC). All fields feature two local maxima, centered approximately at the 20°N latitude and separated by the Philippines–Taiwan meridian. TCs in CCLM-NCEP aggregate most densely in the main development region ($10^\circ\text{--}30^\circ\text{N}$, $120^\circ\text{--}150^\circ\text{E}$), located on the east side of the north Philippines, and to smaller extent on the west side. These regions are very well collocated with the local maxima in the CMA and JTWC datasets. Spatial agreement is weaker with the JMA data set. For this data set the highest concentration is distinctively shifted northward, located north-east from Taiwan. Regarding the TC's concentrations all the BTD sets have their own, small distinctive features. For example: the CMA dataset shows the highest concentration in the South China Sea; TCs in JMA aggregate mostly in the north part of the main development region, north-east of Taiwan ($20^\circ\text{--}30^\circ\text{N}$); while in JTWC, TC occurrences are distributed more uniformly between these regions. Additionally, the JTWC track pattern is slightly longer than in other datasets, since TC genesis in this data set is shifted towards tropical areas

of the central Pacific. This is most likely caused by differences in monitoring practices, which were applied to identify and record storms in an earlier stage of development. Other discrepancies are possibly caused by the differences in the available observational sources, techniques and postprocessing practices employed to compile the data sets (Barcikowska et al. 2012; Song et al. 2010).

Overall, simulated CCLM-NCEP TC occurrences appear fairly realistic when compared with BTD features. Taking into account the location of maximum TC aggregation, simulations seem to be most consistent with the JTWC data, though the simulated ratio in the main development region is slightly higher.

Both simulations successfully reproduce the BTD patterns of spatial variability—associated with ENSO (Camargo et al. 2007; Wang and Chan 2002). Contours shown in Fig. 1 indicate the difference between years with the positive and negative ENSO phase, derived from the observation-derived and simulated TC trajectories. The patterns in all simulated and BTD fields show characteristic anomalous TC activity in the south-eastern quadrant of the WNP during the positive phase and in the north-western quadrant during the negative phase. This spatial modulation of TC trajectories, as well as its impact on lifetime and TC maximum intensity, is the most distinguishable feature of the recorded interannual TC variability over the WNP (Camargo and Sobel 2005; Chan 2000; Wang and Chan 2002; Wu et al. 2012). Nevertheless, not many modeling studies (Zhao et al. 2007; Emanuel et al. 2008) till now have shown a reasonable skill in reproducing interannual variability of TC frequency in this region.

High skill of CCLM in reproducing the spatial distribution of TCs as well as the spatial and temporal sensitivity of TC variations to ENSO, stems largely from skillful simulation of the large-scale circulation over the WNP. This has been achieved with an application of a spectral nudging technique. Feser and Barcikowska (2012) have shown that the technique substantially reduces both the simulated positive bias of the Asian monsoon circulation (e.g. westerly winds, relative vorticity and precipitation) and the negative bias of the subtropical high. The study also shows, that nudging the simulated large-scale winds towards the reanalyzed atmospheric state, allows for detailed replication of the observation-derived TCs. In other words, simulated TC trajectories very closely followed, in both space and actual time, their BTD counterparts.

This agreement is also reflected in an actual location and time of storm intensification, which results in a pattern of the mean TC intensity, which is very similar to the BTD pattern. Figure S1 shows spatial distributions of mean TC intensity with a characteristic local maximum in the subtropical area between Taiwan and Japan. This feature is associated with the impact of TC contraction and intensification during TC recurvature, which usually occurs in the

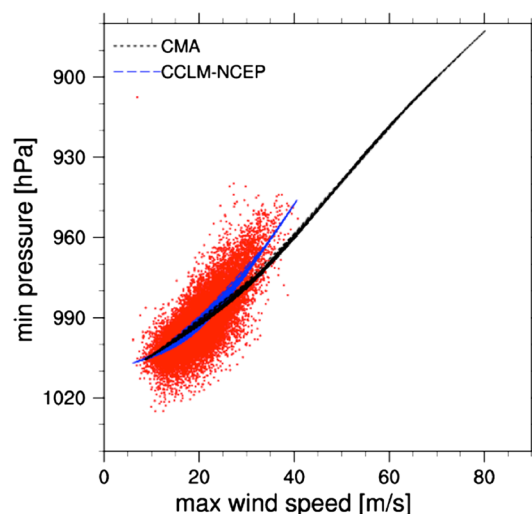


Fig. 2 Scatterplot of maximum surface wind speed (m s^{-1}) versus minimum pressure (hPa) for all TC 6-h occurrences during their lifetime in the period 1978–2010, simulated with CCLM-NCEP (red dots). Blue and black lines are cubic spline fits for CCLM and for CMA BTD, respectively

vicinity of Taiwan. Nevertheless, simulated mean intensity per storm is much weaker than the BTD values, and this issue will be discussed in the following.

Cha et al. (2011) suggested that spectral nudging of the models interior towards the large-scale atmospheric state inhibits the TC intensification process. In contrast, Feser and Barcikowska (2012) found, that in a 50-km horizontal resolution run the impact of the spectral nudging on TC wind speed is negligible. This is due to other limiting factors, consistently with other studies (e.g. Knutson et al. 2007; Wu et al. 2014), which are mostly associated with model dynamical characteristics, such as horizontal resolution or the convection scheme.

The 6-h intensities, simulated with CCLM-NCEP for the 1978–2001 period, are shown in Fig. 2 in the form of a wind–pressure relationship. Both maximum wind speeds and minimum core pressure are severely underestimated, reaching the Saffir–Simpson category 4 (<920–944 hPa) in terms of minimum core pressure, but only the lower limits of Saffir–Simpson category 2 (>43–49 m/s) in terms of maximum surface wind speed. A strong underestimation of the winds already occurs when pressure drops below ~980 hPa. The strong nonlinearity in the simulated wind–pressure relationship (blue line), compared to the BTD one (black line) is a characteristic deficiency of a ~50 km resolution model, as the resolution is not sufficient to resolve the strong pressure gradients that intense TCs feature (e.g. Knutson et al. 2007; Wu et al. 2014). Wu et al. (2014) has explicitly shown that this deficiency certainly impacts a distribution of TC intensity and consequently underestimates the number of intense TCs. Close inspection of the

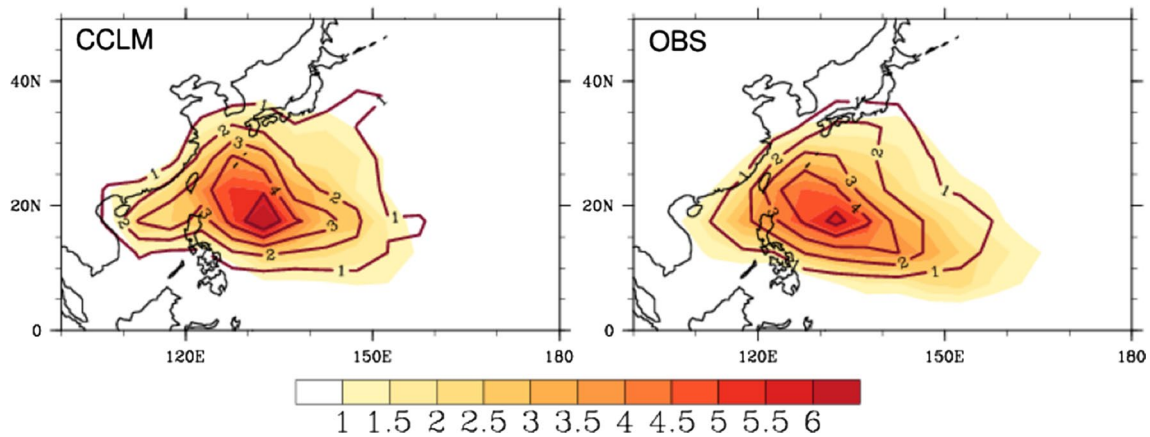


Fig. 3 Density (shaded) of intense TC 6-h occurrences (falling into category 2–5 on the Saffir–Simpson Hurricane Scale), normalized by their spatial mean for *left*) CCLM-NCEP (shaded) and CCLM-ERA (contours) simulations and *right*) observations: JTWC (shaded) and

JMA (contours) for the common period: 1978–2001. Numbers are shown for $5^\circ \times 5^\circ$ lat-lon boxes. Sample of the intense TCs in CCLM was derived with non-objective criteria, matching the observed frequency number of intense TCs

simulated CCLM storms (Feser and Barcikowska 2012; Feser and von Storch 2008a, b) has shown additionally, that the model can adequately reproduce the time and trajectory of intense storms, except that its intensity category is often too low. This shortcoming strongly indicates, that intensity measures alone cannot serve as a benchmark for the extraction of a realistic sample of the intense storms. We take this fact into account in the further part of our analysis, which focuses on the climatology of intense TCs.

3.2 Simulated and observed temporal variability of TCs over the western North Pacific

This section presents results derived for all and intense TCs in JASON seasons of 1978–2010. Due to the model deficiencies in representing realistic intensities, as described above, derivation of the intense TCs is not based on objective criteria. In order to reconstruct climatologies of intense TCs, the tracking settings were tuned to match higher intensity thresholds, but also to match the observed frequency of intense TCs. In exact terms, we have chosen the number of TCs from the upper tail of the intensity distribution, which corresponds to the number of TCs within category 2–5 of the Saffir–Simpson classification. Since the tracking algorithm sometimes captures weaker TCs, the number of detected TCs (seasonal mean: 7.68 TCs in CCLM NCEP, 6.6 TCs in CCLM ERA for 1978–2001) in the reconstruction is slightly larger than the JMA and CMA numbers (seasonal mean: 6.03/6.8 TCs), but distinctively smaller than the frequency in JTWC (9TCs). This discrepancy stems most likely from a different definition of the maximum intensity used in JTWC, 1-min sustained wind speed, in contrast to the other weather agencies using the WMO-recommended 10-min averaging period (Barcikowska

et al. 2012; Kamahori et al. 2006). The standard deviations for the simulated and BTD annual TC variability are both relatively similar to one another: 2.9/2.5 TCs for CCLM-NCEP and CCLM-ERA respectively, and 2.2/2.3/2.7 for JMA/CMA/JTWC. The skill of the chosen tracking algorithm settings is high enough to capture very realistically the climatological features of the spatial density, an interannual and decadal scale variability of the intense TCs and their relationship with the large-scale circulation.

Figure 3 shows the spatial density, derived from hind-casted (CCLM-NCEP, CCLM-ERA) and BTD (JTWC and JMA) intense TCs' 6-hourly trajectories between 1978 and 2001. The simulated TC occurrence ratios are very realistic compared to BTD. The pattern is consistent with the usual trajectories of the intense TCs. It spreads from the south-eastern part of the WNP, where most of TC genesis occurs, and recurves towards Japan. The simulated intense TCs aggregate most densely in the main development region (20°N , $120^\circ\text{--}150^\circ\text{E}$). Both CCLM-NCEP and CCLM-ERA exhibit maxima in the region (20°N , $130^\circ\text{--}140^\circ\text{E}$), which matches almost perfectly all the BTD. The JTWC track pattern is slightly longer than those of the three datasets, since TC genesis in this dataset is shifted towards tropical areas of the central Pacific. This is most probably caused by differences in monitoring practices, which were applied to identify and record cyclones in an earlier development stage.

We wish now to examine interannual, decadal and longer-term variability of the simulated TCs. Following the convention of our analysis we will compare first the simulated and observed features in the most recent period, from 1978 to 2010. Figure 4 presents time series of the simulated and BTD seasonal (JASON), basin-wide TC activity metrics: counts of TCs with at least tropical

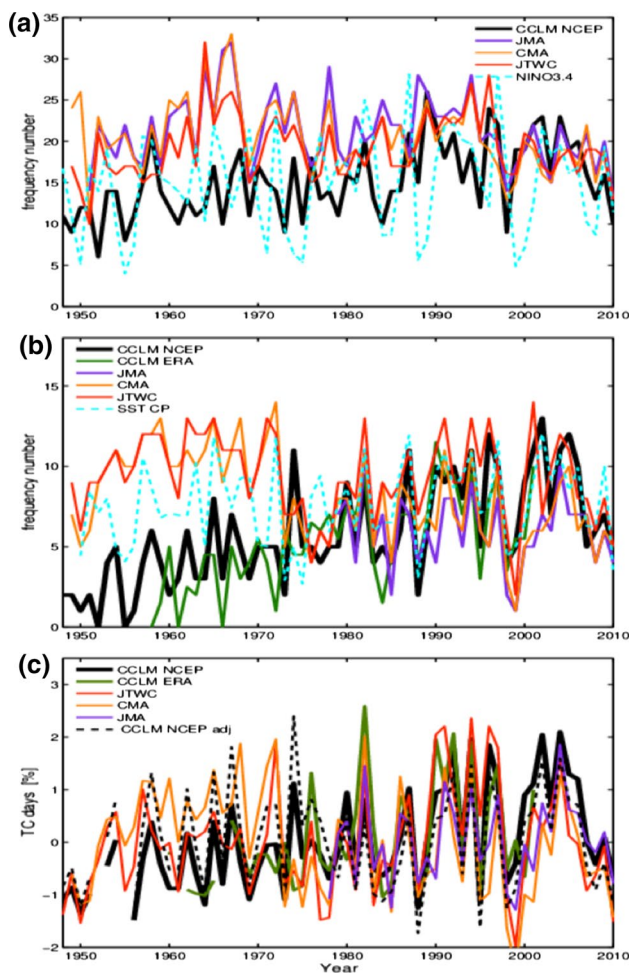


Fig. 4 Seasonally (July–November) aggregated numbers of **a** TCs of wind intensity higher than 17 m s^{-1} **b** intense TCs (qualified as category 2–5) and **c** normalized to unit variance anomalies of intense TC day numbers. Anomalies were derived in reference to the mean of the period 1978–2010. Time series were derived from CCLM simulations forced with atmospheric reanalyses: NCEP-NCAR, ERA-40 (CCLM NCEP, CCLM ERA, respectively) and from BTM sets (denoted as JMA, JTWC, CMA) for the intense TCs. JMA provides TC intensity estimations only since 1978. Anomalies in ‘CCLM NCEP adj’ were derived separately for the periods 1948–1978 and 1979–2012 to account for the difference in standard deviation between those periods. Time series of **a** NINO3.4 index and **b** SST anomalies in the tropical Central Pacific (0° – 10°N , 180° – 160°W) were rescaled according to the TC time series

storm intensity ($>17 \text{ m s}^{-1}$), intense (category 2–5) TCs, and the lifetime of the intense TCs.

For 1978–2010 metrics for the tropical storms (Fig. 4a) show a weak correspondence between the BTM and simulated data sets. Simulated numbers are smaller than observed ones till the late 1990s. These numbers converge in the early 2000s. A relatively weak relationship in the interannual to decadal variations before the 2000s adds to the generally low agreement, reflected in

the correlation coefficients of 0.31, 0.34 ($\alpha = 10\%$, for JMA and JTWC, respectively).

It is also worth noting that the BTM data sets have a wide range of uncertainty, showing relatively high correlation coefficients ($r = 0.74, 0.76$, $\alpha = 5\%$ for JTWC vs JMA and JTWC vs CMA, respectively) for the storm counts, but much weaker correlations for the metrics including tropical depressions (e.g. $r = 0.38, 0.42$, $\alpha = 5\%$ for JTWC vs JMA and JTWC vs CMA respectively). Moreover, only CCLM simulations exhibit a positive relationship between basin wide TC numbers and ENSO, sharing with NINO3.4 index a correlation of 0.23 (not significant at $\alpha = 5\%$) for 1978–2010, and of 0.29 (significant at $\alpha = 5\%$) for 1948–2010. In contrast, BTM show very small and not significant correlations. This calls into question their quality and ability to serve as a reference dataset (Song et al. 2010) to reconstruct a physically meaningful TC climatology.

The interannual variability of intense TCs (Fig. 4b, c) shows much better than tropical storm counts an agreement between simulations and BTM. For the period 1978–2010 the frequency of the intense TCs in CCLM-NCEP shows significant ($\alpha = 1\%$) correlations with all BTM: 0.41, 0.51, 0.62 for CMA, JMA, JTWC respectively. Further examination indicates that the strong correspondence between these datasets is caused by their strong relationship with ENSO. The data sets exhibit significant ($\alpha = 1\%$) correlation coefficients of 0.51, 0.61, 0.56, 0.43 for CCLM-NCEP, JMA, CMA, JTWC, and 0.55 for CCLM-ERA ($\alpha = 1\%$, for period 1978–2001) with NINO3.4 index. The correlation between CCLM simulations and SST in the equatorial Central Pacific (0° – 10°N , 180° – 160°W) is even higher (0.77 for the CCLM-NCEP and 0.72 for CCLM-ERA ($\alpha = 1\%$, for 1978–2001), suggesting local SST is a robust proxy for the variability of intense TCs.

The derived strong statistical relationships will be corroborated in the next section, with an analysis of physical consistency between TC variability and large-scale environmental patterns. This is an important improvement compared to other regional reconstructions (Wu et al. 2014), which show rather low sensitivity to large-scale environmental conditions such as ENSO and consequently, a low agreement between the observed and hindcasted interannual TC variability.

In terms of longer-term variations during the 1978–2010 period, metrics for all data sets are broadly consistent, indicating increasing tendencies in the 1970s–1990s period and lower values/or no tendencies in the 2000s. For example, the frequency of the intense TCs exhibits the most pronounced increase in CCLM-NCEP and JTWC, showing linear trend coefficients of 2.4 and 2.0 TC/decade in 1978–1998 (Fig. 4b), CCLM-ERA and CMA indicate much

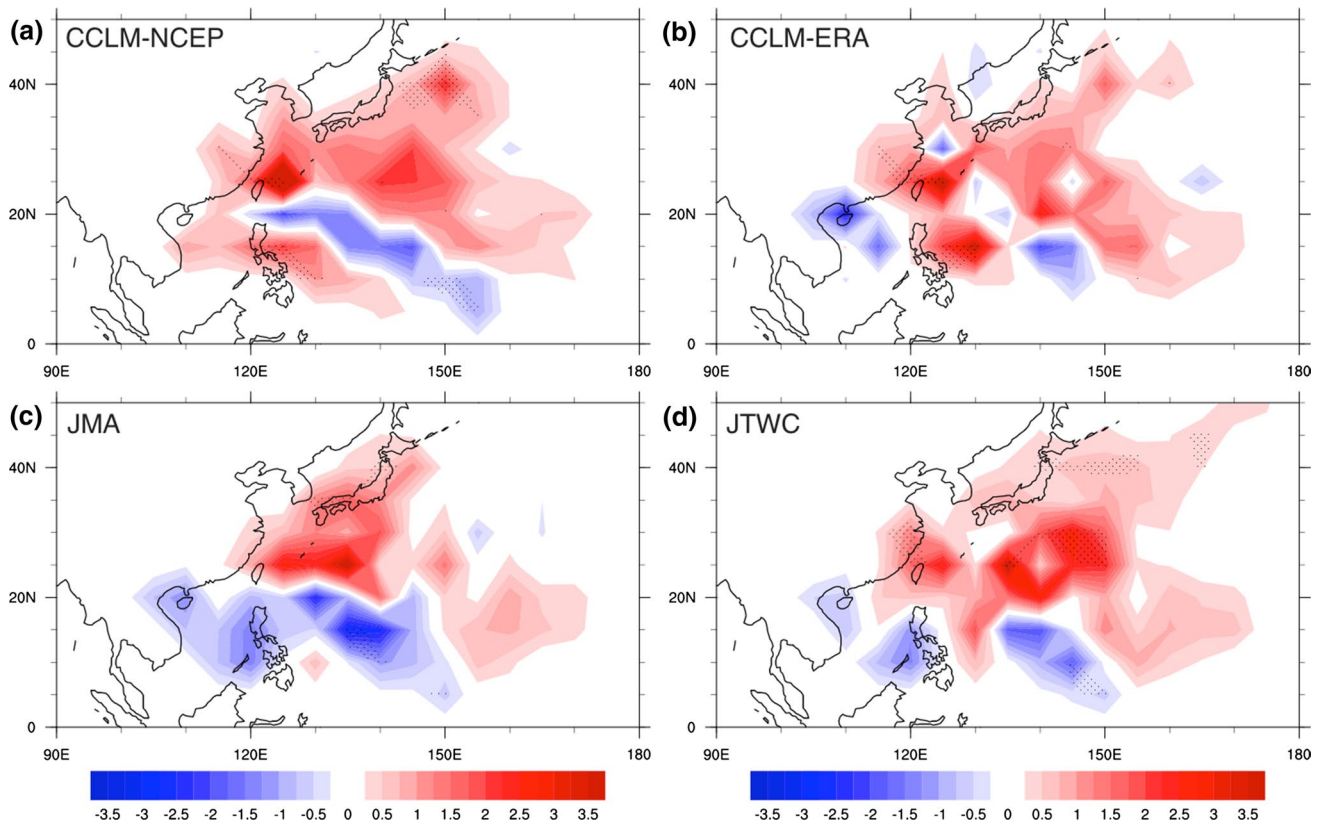


Fig. 5 Linear trends of TC activity for seasonally (JASON) accumulated 6-h occurrences of intense TCs, in the period 1978–2001. Trends are estimated using linear regression for every $5^\circ \times 5^\circ$ grid

box; for **a** CCLM-NCEP, **b** CCLM-ERA, **c** JMA, and **d** JTWC. In addition, trends were multiplied by a factor of 10, to signify a change per decade

smaller changes (1.2, 0.4 TC/decade). This apparently large spread between the derived trends is partly associated with the large interannual variability and the relatively short length of the analyzed period. These features limit the accuracy of the estimations and require special caution when interpreting the results.

The regional features of the derived trends (Fig. 5) show also a general agreement between the data sets. Trend coefficients, derived for the number of TC occurrences in 1978–2001, show an increase in the number of TC days over East Asia (in the vicinity of Taiwan and Japan) and a decrease to the southwest, indicative of a north-eastward shift of TC activity. This spatial shift is less pronounced in JMA (Fig. 5c), where the area with negative trend spreads eastward across the South China Sea and the Philippines, and effectively cancels out positive tendencies. The JTWC and CCLM simulations are dominated by positive tendencies, however with negative tendencies for TC passages east from the Philippines.

The long-term trends (Fig. 4b, c) reconstructed over six decades (1948–2010/1959–2001 for CCLM NCEP/CCLM ERA) differ substantially from the BTD trends. This discrepancy stems from a very low agreement between BTD

and simulations in the pre-satellite era (1948–1978). In this period all metrics derived from CCLM simulations, indicate remarkably lower TC activity than available BTD (CMA, JTWC). Consequently, both simulations exhibit pronounced positive tendencies for TC activity. For example, regression coefficients derived for the intense TCs are 1.25, 1.33 TC/decade for CCLM-NCEP and CCLM-ERA, respectively. In contrast BTD show strong multidecadal variations, with minima located in the late 1970s and maxima in the mid-1950s–1970s and 1980s–2000s. These variations are accompanied with either stronger (-1.43 TC/decade for CMA) or weaker (-0.36 TC/decade for JTWC) negative tendencies. It is also worth noting that similar multidecadal variations are present in the time series of the equatorial Central Pacific SST (0 – 10° N, 180 – 160° W, Fig. 4b). The apparent lack of consistency between the long-term changes in simulated TCs and local SSTs substantially reduces correlations from $r = 0.77$ in the 1978–2010 period to $r = 0.53$ in 1948–2010.

On the other hand, the time series of the CCLM-NCEP metrics, adjusted to the different mean and magnitude of variance between pre-satellite and the latter period (Fig. 4c, CCLM-NCEP adj), also exhibit multidecadal variations.

CCLM-NCEP adj time series, in which the long-term trend is removed, shows local maxima in the mid1950s–1970s and the mid1980s–2000s. This corresponds better with the variations in the observed regional SSTs (i.e. tropical Central Pacific) and TCs.

It is worth noting that these multi-decadal TC variations, as well as associated large-scale SST and atmospheric circulation changes in the tropical Pacific, were reproduced in another modeling study (Matsuura et al. 2003). This study employed a coupled GCM model, which is forced with daily mean SST and atmospheric fluxes only. This is an important difference in comparison to our experimental design, where the climate is strongly nudged towards the observed SST and large-scale atmospheric state. A consequence of that difference could be an apparent discrepancy between the multidecadal TC variations, simulated in Matsuura et al. (2003), and the strong upward trend simulated by CCLM. The logic behind that relates to the limited quality of the reanalyzed atmospheric circulation, which influences the simulated CCLM TC climatology. Potential misrepresentations of the atmospheric state in the pre-satellite era could lead to temporal inhomogeneities, manifested in the derived long-term TC trend. This possibility will be investigated later in the study.

3.3 Physical relationship between spatio-temporal variability of intense TCs and large-scale environmental patterns

In this section we examine the derived CCLM climatology of the intense TCs in terms of the physical link between intense TC variability and large-scale environmental patterns. First, we use EOF analysis to extract dominant components of varying TC density. Isolating decadal time scales of TC variability and associated large-scale environmental patterns is done with SSA and MSSA analysis. SSA is applied to the time series of basin wide seasonal number of intense TC days. MSSA—the multivariate version of the former—is applied to isolate spatially coherent temporal patterns from the SST and SLP fields.

Results of the EOF analysis are presented in Fig. 6, which describes the first component (EOF-1) of the BTD and simulated variability in terms of their spatial and temporal features. The contribution of EOF-1 unambiguously dominates over the other remaining modes of variability, explaining 20% in CCLM-NCEP and 16, 21, 22% in JTWC, CMA and JMA of total TC density variance from 1978–2010. EOF-1 exhibits a striking similarity between observation-derived- and model-based results, both in terms of spatial pattern and temporal evolution.

The pattern (Fig. 6b) represents the main features of the intense TCs' tracks. Positive loadings of all EOFs spread from the south-eastern quadrant of the WNP, where most

of TC genesis occurs, and extend toward the Asian coast or recurve towards Japan. The pattern in JTWC is exceptionally elongated towards the south-east, which most likely stems from different operational practices. As discussed in the previous section, these practices involve recording cyclones in their earlier development stage, which results in storm genesis shifted towards the tropics.

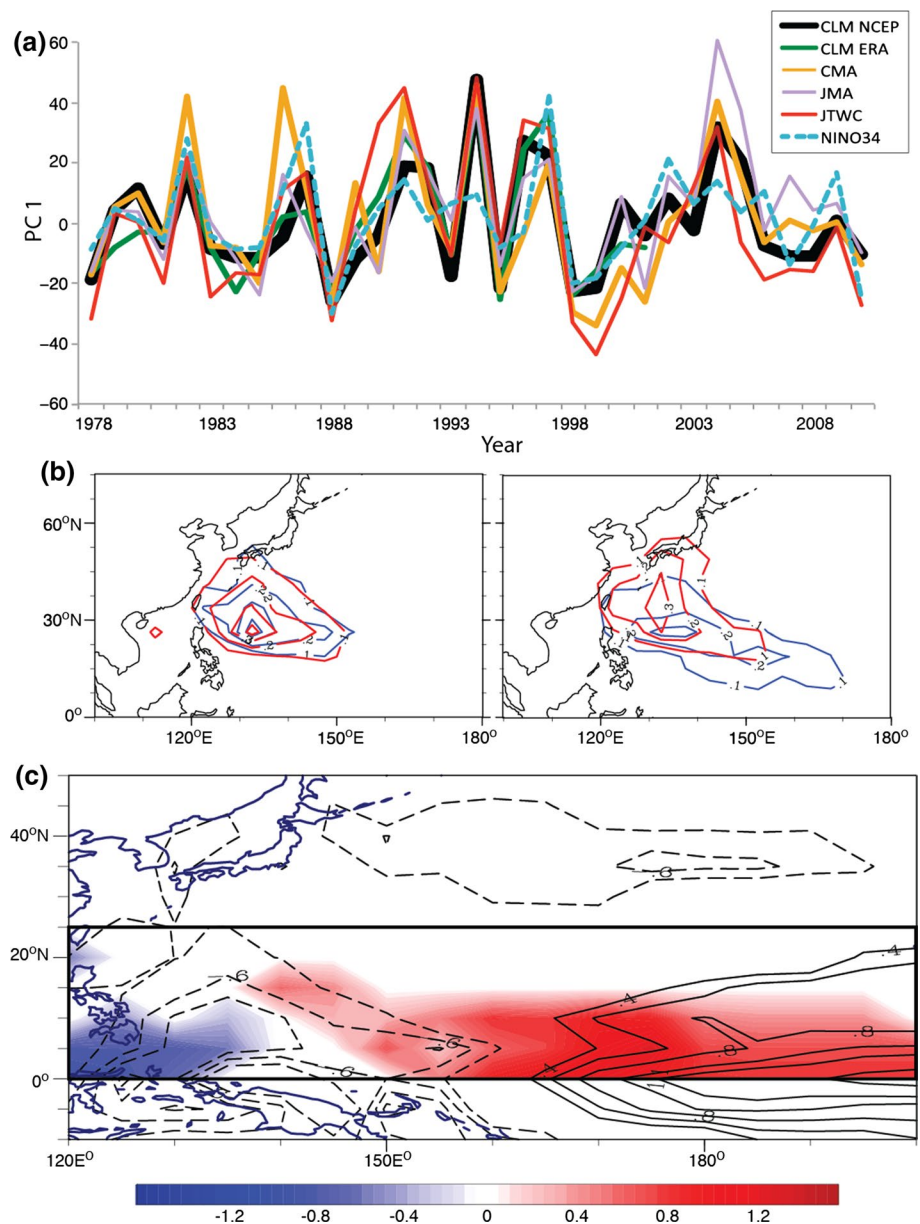
All the time series (PC1) of the EOF-1 component share notably high correlations. Time series of CCLM simulations overlap each other for most of the 1978–2001 period, and have a correlation coefficient of 0.91. Smaller, but still substantial correlations exist between CCLM-NCEP and BTD for the 1978–2010 period, 0.74 for CMA, 0.79 for JTWC and 0.81 for JMA.

These time series also follow very closely the NINO3.4 index, indicative of a relationship with ENSO. Substantial and significant ($\alpha = 5\%$) correlation coefficients are found for all data sets, 0.63 and 0.69 for CCLM-NCEP, and CCLM-ERA (1978–2001) simulations, and 0.54, 0.65, 0.67, for JMA, CMA and JTWC, respectively. Further analysis shows also that spatio-temporal features of the derived component are physically consistent with the variability of the large-scale environmental patterns. We focus here on the fields of SST and the GPI index, which incorporates both CCLM SST and atmospheric fields. This choice is justified by many studies (e.g. Camargo et al. 2007), showing large-scale SST patterns and GPI to be the most relevant proxies for studying environmental impacts on TC variability. A regression of SST and GPI index (Fig. 6c) on simulated intense TC variability over the WNP exhibits typical patterns associated with ENSO phenomena. Anomalously high TC activity in the main development region is associated with positive SST anomalies in the eastern part of the tropical WP, while negative anomalies are more confined to the western parts of the tropical WP, the South China Sea and Kuroshio Extension region. Consistent with these anomalies are anomalies in the large-scale atmospheric circulation, resulting in environmental conditions being more favorable for TC genesis (positive GPI anomalies) in the south-eastern quadrant of the WNP than in the western part (negative GPI anomalies).

These results agree well with the observational findings (Wang and Chan (2002); Camargo and Sobel (2005); Kim et al. (2010)), demonstrating the effect of ENSO on modulation of TC genesis location and consequently storm persistence, length and intensity. Our analysis shows, together with other regional downscaling studies (Mei et al. 2015), that above-normal SST over the tropical Central Pacific and the associated atmospheric circulation are primary drivers of not only spatio-temporal variations of TC density but also interannual counts of TC variability.

In the next part we examine the decadal-scale variations of TC variability and their association with

Fig. 6 Time series **a** and spatial patterns **b** of the first EOF (PC1) of the intense TCs variability (May–November): (*left*) CCLM NCEP (*blue*) and CCLM ERA (*red*) simulations; and (*right*) BTD sets JTWC (*blue*) and JMA (*red*). NINO3.4 index for the season May–November was rescaled by a factor of 100. PC1 explains 20.4, 34.5, 16 and 22.3% of total variance in CCLM NCEP, CCLM ERA, JTWC, and JMA TC total variance. It also shares correlation (coefficients $r = 0.63, 0.69, 0.65, 0.67$) with the NINO3.4 index. **c** Regression of seasonal (July–October) SST (*black contours*, negative values are *dashed*), and GPI index (*shaded*), computed from CCLM-NCEP simulation variables on NINO3.4 index. GPI and SST were normalized to zero mean and unit variance. Only values significant at the alpha 10% level are shown



environmental conditions. In order to extract a decadal-scale signal of the observation-derived and simulated TC activity we analyze them with SSA, which is a time-scale selective method. A robust separation of the time scales requires a sufficiently long dataset; therefore we have chosen the longest available records (1948–2010), namely CCLM-NCEP, JTWC and CMA. Nevertheless, the length of these datasets, especially in the presence of potential inhomogeneities, cannot guarantee robust, significant results. This will require further analysis, which involves alternative and preferably longer datasets. Therefore following the analysis of TC variability we will apply MSSA to the meteorological fields in the NCEP-NCAR reanalyses within the CCLM model domain and the 20CR reanalyses for the Pacific region.

The results have shown that all analyzed TC, SST and SLP data sets consist of three dominant components. Those components represent long-term, decadal and also interannual variability, associated with previously analyzed ENSO impacts. Although a decadal component is present in all analyzed data sets, its signal in JTWC and CCLM simulations in the pre-satellite era is less distinguishable. This again points to the problem of quality and inhomogeneities obstructing the signal in TC records, which turns our primary attention to the recent—1978–2010—period, when observations are more reliable.

Figure 7a shows time series of the seasonal TC days anomalies (with trend removed) in CCLM-NCEP, JTWC and CMA and their reconstructed decadal component (RCs). The RCs explain a substantial amount of the total

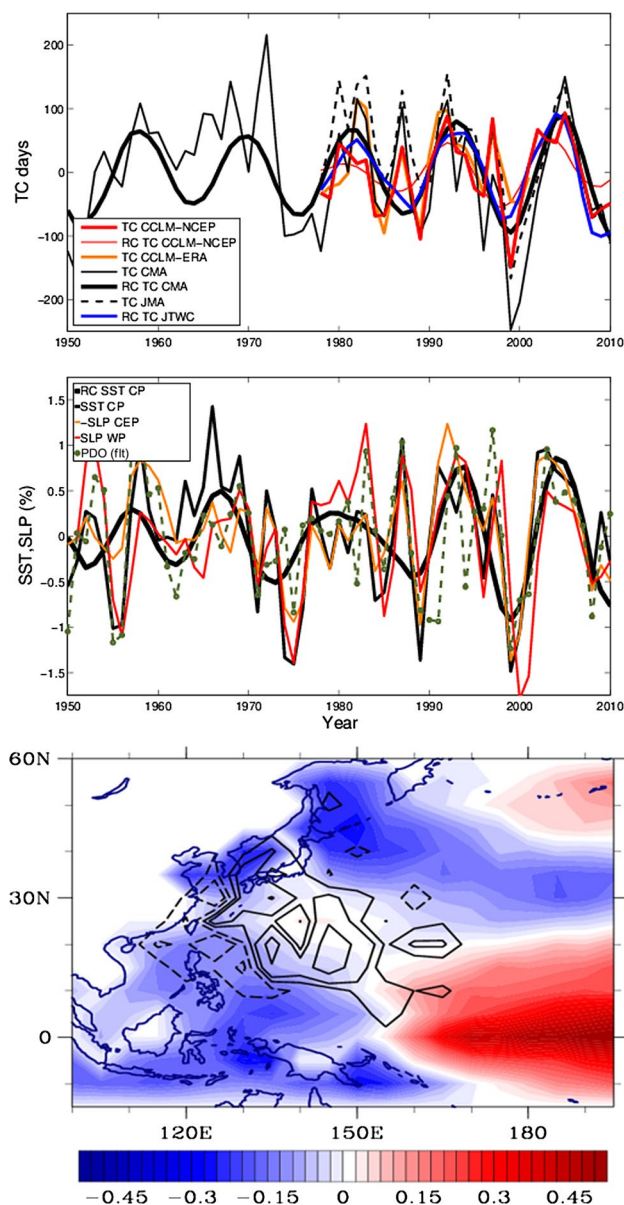


Fig. 7 **a** Time series of seasonal (June–October) TC days in CCLM-NCEP, CCLM-ERA, CMA and JTWC and their reconstruction with the decadal component (RC TC CCLM-NCEP, RC TCCMA, RC TC JTWC). TC days are shown with the long-term trend component (also estimated by MSSA) removed. **b** Reconstructed regional time series of the decadal component of annual SST anomalies (%) in the tropical Central Pacific (CP, 0°–5°N, 180°–160°W) and SLP anomalies (%) in the tropical Central-Eastern and Western Pacific (CEP, 10°S–10°N, 160°–130°W; WP, 20°S–20°N, 105°–135°E). PDO index (PDO fit) is shown with the long-term trend component (also estimated by MSSA) removed. **c** Spatial pattern of the reconstructed SST component (RC SST), during warming phase (positive phase) in the tropical Central Pacific. Values show SST changes within half the 12 years cycle (unit: deg C/6 years). Contours show the corresponding spatial pattern of TC anomalies. Pattern represents the difference between the positive and negative RC SST phase (RC2 SST positive–RC2 SST negative) derived for the yearly anomalies in TC 6 h-occurrences fields. Contours with negative values are *dashed*

variance, i.e. 20, 25, 29%, respectively. Therefore they are easily distinguishable in the TC time series after filtering out the interannual variability contribution (using a 2-year running mean filter). The time evolution of all RCs is almost identical. They contribute remarkably to the observed and simulated anomalously high TC days in the 1980s, early 1990s and mid-2000s. It is worth noting that decadal variations in CMA are also distinct in the pre-satellite era, explaining 21% of the total variance for the whole period (1949–2010).

The following results show that the decadal variations of TC variability, apparent in all TC data sets, are physically consistent with the changes in the large-scale patterns of SST and SLP over the WNP and also in the North Pacific. Application of MSSA to SST and SLP fields in NCEP-NCAR reanalysis isolates their decadal variations (~11–12 years), over the WNP. For the SST, the component manifests mostly in the tropical Central Pacific. It explains 37% of the variance, after filtering out (with a 3-year running mean filter) high-frequency variations. However, without the filtering, RC SST explains only 16% of the variance, which acknowledges the importance of interannual variations in this region.

Figure 7c shows the signature of the component during its warm SST phase in the tropical Central Pacific. Warm SST anomalies along the equator are accompanied by cold anomalies in the Kuroshio Extension and coastal regions, which closely resembles the signature of the warm phase of decadal-scale ENSO (El Niño) or PDO/IPO. This similarity also explains why the time series of the reconstructed RC SST component are in a reasonable agreement with the PDO index. For example, the RC SST time series in 1978–2010 share with the PDO index a significant ($\alpha = 1\%$) correlation of $r = 0.42$. Nevertheless, the PDO index, which is derived from standard EOF analysis, captures much more variability across annual-to-multidecadal time scales and thus its physical significance is still contested (Newman et al. 2016).

Close inspection of the SST and SLP time series (Fig. 7b) shows that their strong and significant anticorrelation ($r = -0.78$, $\alpha = 1\%$) in the tropical Central Pacific (CP), is to a large degree determined by the reconstructed decadal variability. The reconstructed decadal SST changes (RC SST CP) for this region and annual time series of SLP (SLP CP) share a correlation of $r = -0.54$. Additionally, a tight relationship of atmospheric circulation between the tropical Central and West Pacific ($r = -0.55$, $\alpha = 1\%$) as well as substantial correlation between decadal RC SST CP and annual SLP in the Western Pacific ($r = 0.41$) indicates the presence of large-scale coupled ocean–atmosphere climate variability.

These changes are well synchronized and physically consistent with the decadal TC variability, and strongly resemble the typical impact of ENSO. Figure 7c shows the difference between CCLM-NCEP TC density fields during the RC phase with warm SSTs in the tropical Central Pacific and the opposite phase. It captures directly the eastward/westward shift of TC trajectories during phases with warm/cold SST anomalies in the tropical Central Pacific. Following this relationship, decadal-scale warm SST CP anomalies are consistent with an eastward shift of TC genesis, longer TC lifetime, and consequently the anomalously high number of TC days observed and simulated during the early 1980s, mid-1990s and mid-2000s.

Further analysis confirms the presence of the significant, decadal component in a longer meteorological time series and over most of the Pacific region (60°S–60°N, 100°E–80°W). The decadal variations, extracted from the 20CR dataset, substantially contribute and physically link the SST and atmospheric variability in the Pacific domain. These results depict the whole subtropical-tropical Pacific climate as a potential pacemaker for decadal TC variations in the WNP.

Figure 8 shows that both spatial pattern and time series of the decadal variability agree well with the component derived from the 20CR reanalyses. Time series of the SLP in the tropical West Pacific and SST in the tropical Central-East Pacific show a very high and significant ($r = 0.71$, $\alpha = 1\%$) correlation, and this partly stems from the large agreement in their decadal variations ($r = 0.66$ for RC SLP WP vs RC SST CEP). These variations explain 28% of the SLP variance in the tropical Western Pacific (WP, 20°S–20°N, 110°–140°E) and 23% of the SST variance in the tropical Central Eastern Pacific (CEP, 10°S–10°N, 160°–130°W), after filtering out their interannual (3-year running mean filter) variability.

The whole spatial pattern closely resembles the typical features of the Interdecadal Pacific Oscillation (IPO), defined in several previous observational and modeling studies (Power et al. 1999; Deser et al. 2004; Meehl et al. 2013). Figure 8a shows that SST anomalies, during the warm SST phase in the tropical central Pacific, extend towards the tropical East Pacific. SLP anomalies exhibit a typical ENSO pressure gradient between Indonesia and the eastern Pacific.

Regression analysis (Fig. 8b) associates these SST and SLP anomalies with the weakening of the zonal pressure gradient and trade winds in the tropical Central Pacific, an eastward shift of convection (not shown) and precipitation. All these are indicative of a Pacific-wide weakening of the Walker circulation during the warm SST phase and the opposite during the negative SST phase.

The derived decadal climate variability component is physically and statistically consistent with the previously

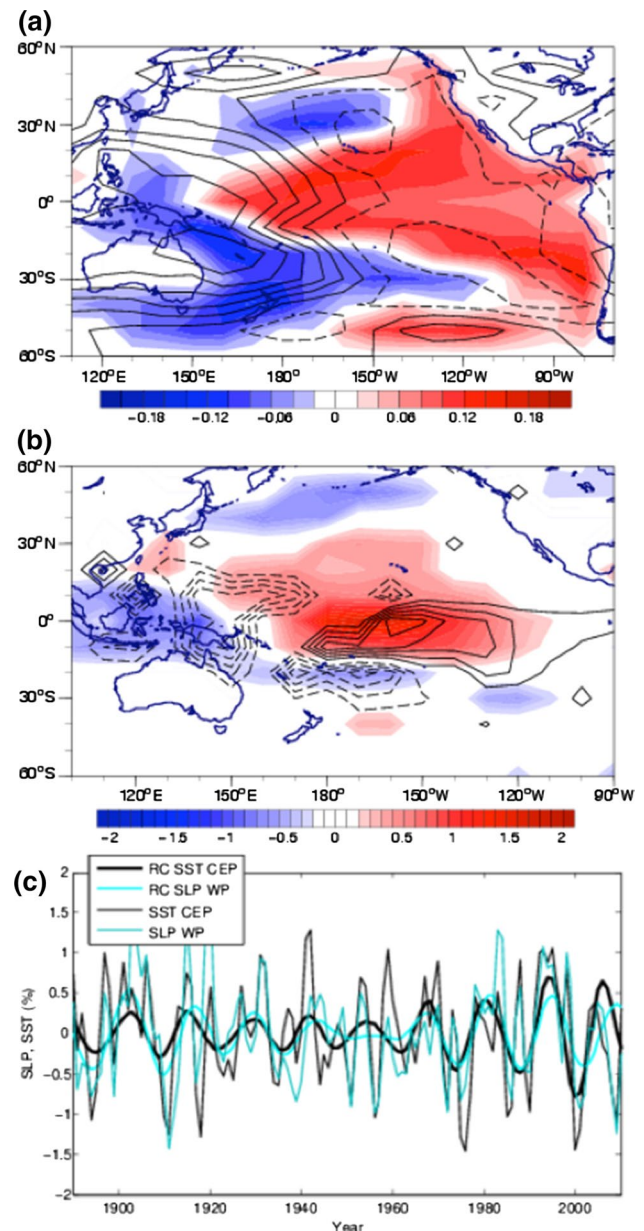


Fig. 8 a Spatial pattern of the annual SST (*shaded*) and SLP (*contours*) components, during the warming phase in the tropical Central-East Pacific. Values show SST and SLP change in unit variance within half the 12 years cycle [$\times 100\%/6$ year]. Contours are -5 to 12.5 with 2.5% intervals and negative values are dashed; b Regression of 20CR annual zonal wind (m s^{-1} shaded) and precipitation anomalies (mm/day , contours) on the annual SLP anomalies (normalized to unit variance), reconstructed with the decadal component in the tropical W Pacific (10°S–10°N, 150°–180°E). Contours are -1.5 to 1.5 with an interval of 0.25 and negative values are *dashed*. The values are significant at $\alpha = 10\%$ level for precipitation, and $\alpha = 15\%$ level for the zonal wind; c Time series of the 20CR SST anomalies (%) for the tropical Central Eastern Pacific (SST CEP; 10°S–10°N, 160°–130°W) and SLP anomalies for the Western Pacific (SLP WP; 20°S–20°N, 110°–140°E) with the multidecadal variations removed, and reconstruction of SST and SLP with MSSA decadal components (RC SLP and RC SST). SST CEP and SLP WP are normalized to zero mean and unit variance, and smoothed with a 2-year running mean filter

shown spatio-temporal variations of both the observed and simulated TC activity. Additionally, the preferential time-scale of the derived component highlights its potential predictive utility for TC activity over the WNP.

Decadal variability of TCs and their association with large-scale conditions over the Pacific region, which are consistent with other papers, studying TC variations on longer timescales, are presented here. Matsuura et al. (2003) found that the observed interdecadal (~20 years period) changes in TC activity over the WNP region in 1951–1999 are tied to the zonal wind, modulation of the trade winds and SST anomalies in the tropical Central Pacific, associated with the wind–evaporation–SST feedback (WES, Xie 1996, Xie and Philander 1994). The observed physical link was corroborated with multidecadal simulations employing a coupled ocean–atmosphere GCM. Liu and Chan (2008) found a similar relationship for the period 1960–2005, but derived from a time series varying on longer time scale. Unfortunately, a relatively short length of the analyzed data set (~40 years) limits the significance of the derived results.

Overall, the CCLM TC climatology shows a realistic and similar to the observed relationship with the large-scale SST and atmospheric conditions, both on internannual and decadal time-scales. This could be used to argue that the reconstructed overall increase of TC activity in the last six decades is driven by long-term changes in climate conditions. On the other hand, several studies (Sturaro 2003; Trenberth et al. 2001) suggest that changing availability of measurements has caused inhomogeneities in atmospheric reanalyses and BTD sets. The CCLM TC climatology may inherit these existing inhomogeneities, because it is forced by large-scale conditions of atmospheric reanalyses. Verifying this issue will be a main goal of the following section.

3.4 Analysis of uncertainty related to the inhomogeneities in the atmospheric reanalyses

Long-term TC climatologies, either derived from BTD or CCLM simulations, may have been impacted by the changing quality and availability of the measurements used in the reconstruction process. Incorporation of satellite measurements since the early 1980s caused (Sturaro 2003; Bassist and Chelliah 1997; Trenberth et al. 2001) remarkable discrepancies in the long-term variability of the upper level atmospheric temperature, represented with different data sets. Vecchi et al. (2013) indicated that most of those data sets (including ERA-40), except for NCEP/NCAR, show no trend. The pronounced cooling in NCEP/NCAR since 1978 is likely an artefact.

High uncertainty in the forcing temperature fields can be a problem for reconstruction of TC climatologies. A modeling experiment by Vecchi et al. (2012) indicated that

upper troposphere temperature influences the development of TC intensity. This supports the hypothesis that the upper atmosphere cooling, found in NCEP-NCAR reanalyses, caused a spurious increase in TC activity in the recent decades, as derived from our CCLM-NCEP simulations (e.g. TC intensity, intense TCs frequency). In the following section we test this hypothesis and investigate the potential impact of inhomogeneities in the atmospheric reanalyses on the reconstructed TC climatology.

Analysis of the seasonal TC counts (Fig. 4b) is not indicating that the cooling trend in the NCEP upper atmosphere has a major impact on the derived long-term TC variability. Both CCLM-NCEP and CCLM-ERA time series show a relatively high agreement since the 1980s, despite the inconsistencies in the forcing temperature fields apparent in this period. This could be related to intrinsic features of the downscaling method. Having a horizontal resolution of 50 km limits the ability of the model to reach realistic intensity values, and consequently limits our ability to detect potential effects of temperature on TC intensification. Therefore we cannot rule out the possibility that this effect becomes more important in higher resolution simulations.

3.4.1 Relation between upper atmospheric temperature and reconstructed TC climatology

In this part, a potential impact of upper atmospheric temperature on CCLM climatologies will be explored from a qualitative perspective. For this purpose, we will analyze the difference between the two simulated TC climatologies (CCLM-NCEP minus CCLM-ERA) and also the difference in simulated atmospheric temperature (T).

Primarily, EOF analysis was applied separately to the vector time series of T differences at 100 hPa, where the differences are most severe (hereafter T100), and differences in the annually accumulated mean TC intensity (intensity, as represented by cubed wind speed, hereafter PDI mean). Additionally, joint EOF analysis was applied to the T100 data set and differences in TC intensity (intensity represented by wind speed, wmax) as well as to T100 and differences in annually accumulated spatial density (spd). Both data sets have different magnitudes of variability; therefore they had to be standardized prior to the analysis.

EOF analysis, applied separately to the vector time series of T differences and differences in the annually accumulated mean TC intensity, suggests no relation between the two data sets. Figure 9a shows time series of T100 and TC intensity differences (RC T100 and RC PDI mean) reconstructed with the first leading EOF modes. RC T100 represents the aforementioned long-term discrepancy, apparent after 1970s in the reanalyses, which explains most (93%, or 84% for standardized

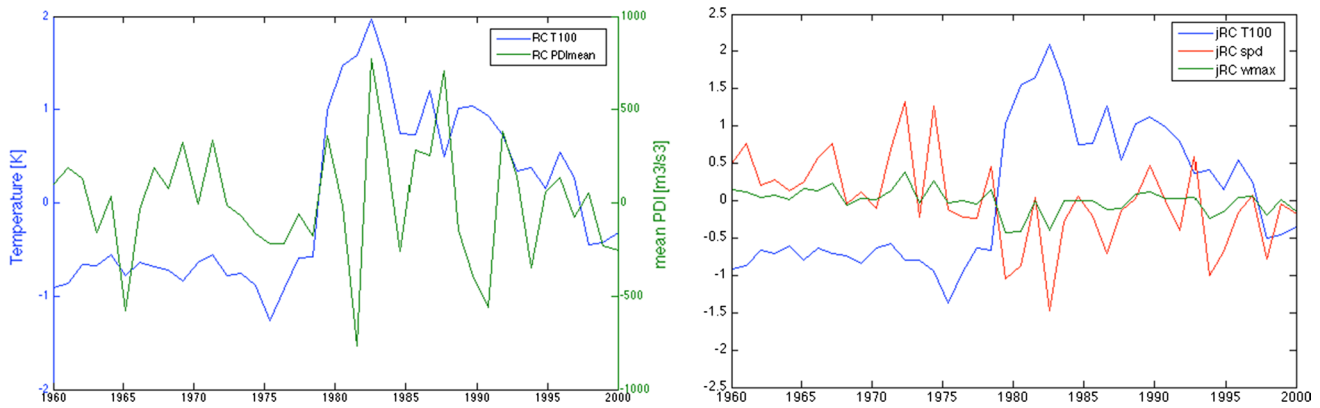


Fig. 9 **a** First components, reconstructed with the EOF analysis, of the differences between CCLM simulations (CCLM-NCEP minus CCLM-ERA) for the temperature (RC T100, *blue*) and mean TC intensity (RC PDI mean, *green*). PDI mean represents differences between simulated annually aggregated, tripled wind speeds. T100 represents differences between atmospheric temperatures at the 100 hPa level. **b** First reconstructed component of the joint EOF anal-

ysis, applied to the differences (CCLM NCEP minus CCLM ERA) in atmospheric temperature (jRC T100, *blue*) and mean TC intensity (jRC wmax, seasonally accumulated wind speed, *green line*) or TC occurrences (jRC spd, seasonally accumulated TC days, *red*). Correlation coefficient between jRC T100 and jRCspd is $r = -0.54$. Reconstructed components (jRCs) are normalized to unit variance

data) of the variance in T100 (CCLM-NCEP minus CCLM-ERA). By contrast, the reconstructed component of PDI mean (RC PDI mean) is far less distinguishable from noise (it represents 16% of the total variance) and is dominated by interannual variability.

The joint EOF analysis suggests that the temperature changes in NCEP-NCAR, might generate a drop in 1970s and a gradual increase afterwards in CCLM-NCEP TC frequency and intensity metrics. Here we extracted a physically consistent component of variability, shared by the differences in temperature (T100) and difference in the number of TC days (hereafter referred to as: spd, wmax). Figure 9b depicts a dominant component (jRC), which has a partial contribution from T100 and from spd (hereafter referred to as: jRC T100, jRC spd) or wmax (jRCwmax) fields. The jRC T100 time series, similar to the previous EOF analysis, describes the abrupt increase of NCEP/NCAR T in the late 1970s and early 1980s, while strong cooling occurs afterwards. The jRC spd and jRC wmax time series manifest a strong drop, followed by decades of gradual increase, associated with similar changes in the CCLM-NCEP TC days and intensity. A remarkable negative correlation between jRC spd (jRC wmax) and jRC T100 ($r = -0.54/-0.50$ for spd/wmax), corroborates physical consistency between simulated upper level temperature and TC activity. Component jRC spd explains 31% of the difference between the simulated TC frequencies. This indicates that upper atmospheric temperature may have an impact on TC climatology and this impact may be even more important in higher-sensitivity applications (higher-resolution experiments).

3.4.2 Impact of changing representation of atmospheric circulation in NCEP/NCAR and ERA-40 reanalyses; analysis adjusting to the potential inhomogeneities

The introduction of satellite-based measurements in the late 1970s might have impacted not only the representation of upper level atmospheric temperatures, but also improved the representation of atmospheric circulation in the atmospheric reanalyses. This improvement, however, must have an effect on the homogeneity of those data sets. The changes in the atmospheric observational systems in the late 1970s are consistent with a shift in variance of TC activity, exhibited in both CCLM simulations. Figure 10 shows the time series (a) and spatial patterns (b) of the leading EOF modes derived from seasonally accumulated TC intensity (PDI, cubed max wind speed) in both CCLM simulations, as well as the time series of annual mean intensity (wind speed) in both reanalyses. The spatial EOF patterns exhibit very similar features. Both patterns indicate that the main contribution to the variance in TC intensity is centered in the region between Taiwan and Japan, which is also the region with the highest mean TC intensity (Fig S2). The temporal evolution of those patterns in both CCLM runs shows a radical increase in variance in the late 1970s. This feature is also recognizable in time series of the reanalyses (Fig. 10) and in the leading EOF (Fig. S1, Supplementary Material) representing the main mode of simulated variability in annual numbers of TC days.

Inhomogeneities manifested by amplified variance of intense TC days since the late 1970s, can impact their long-term statistics and spuriously amplify the derived upward

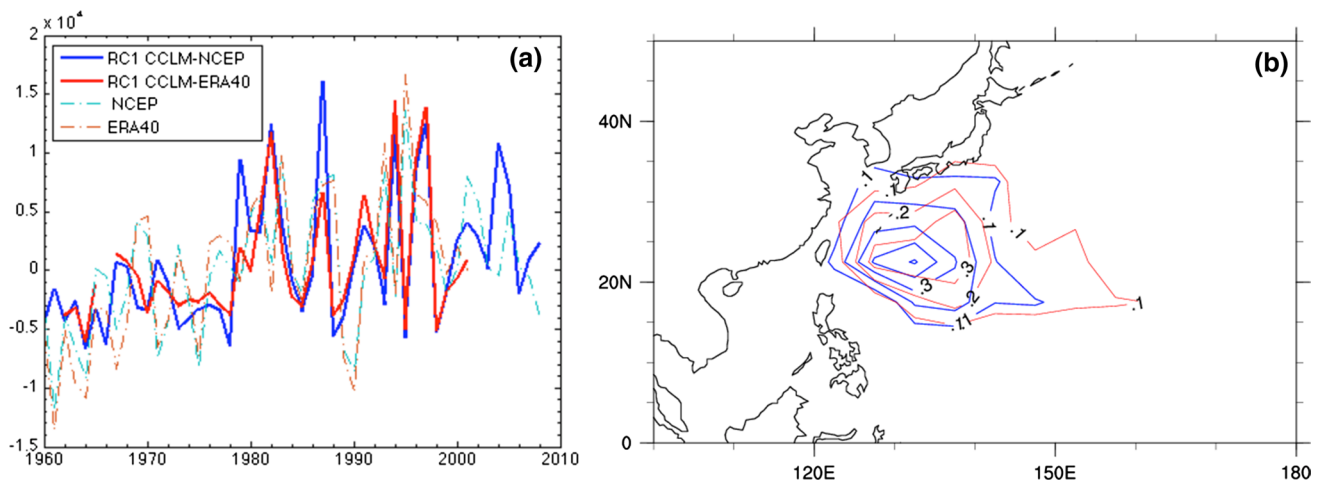


Fig. 10 **a** Time series of the EOF analysis-reconstructed RC1 component of TC intensity fields (annually aggregated tripled wind speed, unit: $(\text{m}^3 \text{s}^{-3})$) derived from CCLM-NCEP (blue) and CCLM ERA (red) simulations. Time series of the wind speed intensity in NCEP

and ERA reanalysis are denoted with stippled blue and red lines. **b** EOF pattern, which represents the main mode of seasonally TC intensity variability in CCLM NCEP (blue) and CCLM ERA (red). EOF was derived for the common period 1961–2001

trend. To remove this potential effect, we adjusted the analyzed time series by normalizing them to zero-mean and unit variance, separately in the pre-satellite (before 1978) and satellite periods. This adjustment (Fig. 4c) removes a long-term trend and amplifies a contribution of multi-decadal TC fluctuations during the last six decades. These temporal features, e.g. positive anomalies in the late 1950s–1970s and in the mid 1980s–2000s, better agree with the observed TC variability (JTWC and CMA BTD), as well as with the multi-decadal SST fluctuations in the tropical Central Pacific.

Given these results, great caution must be used when interpreting long-term trends derived from reanalysis-forced simulations as well as BTD. Deriving realistic TC representations may require us to make some compromises between the two alternative data sets, and to analyze the pre-satellite and satellite periods separately.

4 Summary and conclusions

This study presents two climatologies of tropical storms, that focus on intense TCs, (category 2–5 on the Saffir–Simpson–Hurricane–Scale) in the western North Pacific basin, derived from the last six decades (1948–2012, 1959–2001). These two datasets were reconstructed with a dynamical downscaling approach using the regional climate model Cosmo-CLM with a grid distance of 50 km. The model downscales the weather using prescribed SSTs and interior nudging towards the observed large-scale atmospheric state. Assuming a reliable representation of the observed large-scale atmospheric circulation, we expect the model to provide a reliable and homogeneous representation of the weather at the regional scale.

This approach enabled us to provide an alternative for observations-based TC climatologies, strongly affected by temporal and spatial inhomogeneities.

In this study we downscaled two different atmospheric reanalyses: NCEP-NCAR for 1948–2010 and ERA-40 for the period 1959–2001. These are the longest TC climatologies that have so far been constructed using a dynamical downscaling approach. This allowed us to assess the skill of the model to hindcast TC climatologies, in terms of track patterns, intensity, temporal variations on the inter-annual-to-decadal time scale and their association with large-scale environmental patterns.

The experimental design also enabled us to estimate the uncertainty caused by the different representation of atmospheric state and SST in these datasets, and potential temporal inhomogeneities impacting the quality of the reanalyses.

The first part of the study demonstrates that CCLM is highly capable of simulating TC climatologies in a way that is realistic and comparable with BTD for the recent three decades (1978–2010). Both simulations successfully reproduced the BTD interannual to decadal variability and trends of intense TCs. The spatial distribution of tropical storms as well as their temporal variability exhibits strong sensitivity to ENSO. This applies especially to intense storms reaching at least category 2 (intense TCs). For example 39% of the variance of their number can be explained by the NINO3.4 index and in 59% explained by the SST in the equatorial Central Pacific (0° – 10° N, 180° – 160° W), suggesting that these indices may be a robust proxy for TC activity predictions.

High skill of CCLM in reproducing the observed inter-annual and decadal TC variations is obtained with the

application of the spectral nudging method. This approach facilitates the model to successfully reproduce the atmospheric patterns associated with the ENSO-type SST variations on interannual and decadal time scales.

MSSA analysis allowed us to extract a coupled SST-atmosphere component, which shapes Pacific climate variability on decadal time scales. Analysis of the 20CR dataset indicates, that the component manifests mostly in the tropical SSTs, modulates pressure gradient, trade winds and precipitation, being most likely associated with the fluctuations of the Walker Circulation cell. These Pacific climate decadal variations are consistent with other studies analyzing records and paleo-reconstructions of SST, atmospheric variables, Southern Oscillation index and subsurface ocean variability (Tourre et al. 2001; Brassington 1997; White and Tourre 2003; Luo and Yamagata 2001; White et al. 2003).

We have shown, that the derived decadal variations in the Pacific large-scale circulation are consistent with the east–west shift of TC tracks and TC lifetime, which e.g. contributed to the anomalously high seasonal numbers of TC days in the mid-1990s and mid-2000s. The decadal climate variations in the 20CR dataset reach back to the 20th century. Their presence as well as their statistical and physical link with the basin-average number of TC days, suggests its potential predictive utility on decadal time scales. It is important to note that the 20CR dataset also contains temporal inhomogeneities (Krueger et al. 2013). Therefore the predictive value of the derived Pacific climate component should be confirmed further, preferentially with idealized model experiments.

Analysis of the long-term tendencies of TC activity shows that both CCLM-simulations can reproduce the observed increase of TCs and intense TCs during the period 1970s–1990s and a drop in the 2000s. Nevertheless, the short length of the time series and their large interannual variability led to the large spread between the data sets (e.g. 0.4 TCs/decade for CMA, 2.0 for JTWC, and 2.4 for CCLM-NCEP). The increase in the frequency of the intense TCs in CCLM-ERA (1.2 TC/decade) is substantially weaker than in CCLM-NCEP (2.4 TC/decade). However, due to a strong sensitivity of these trends to the interannual variations, we cannot claim their significance nor attribute them with high confidence to the different representation of reanalyzed atmospheric state such as different trends in the upper atmospheric temperature.

The linear trends of the simulated frequency of intense TCs for the six decades (1948–2010/1959–2001 for CCLM NCEP/CCLM ERA) show a substantial increase, in contrast to the multidecadal variations present in BTD. This discrepancy is likely associated with measurement uncertainties in the pre-satellite era, which may impact BTD and simulated TC intensities in opposite ways. While Landsea et al. (2006) suggested that records of TC intensities are

likely overestimated in the pre-satellite era, we found that the poor quality of the atmospheric circulation in both reanalyses in this period caused an underestimation of CCLM TC intensity and number of intense TCs days during 1948–1978. A pronounced increase in the variance of yearly TC statistics in 1978, consistent with the introduction of satellite measurements, might have amplified the long-term tendencies derived from both CCLM reconstructions.

Additional analysis, which removes the long-term upward trend from CCLM simulations emphasizes pronounced multi-decadal fluctuations of TC activity with local maxima in the 1960s–1970s and mid-1980s–1990s. These multi-decadal TC variations are consistent with BTD datasets. They are also physically consistent with the fluctuations of the large-scale SST pattern in the tropical Pacific, shown previously to be tightly linked with the Pacific atmospheric overturning cell. Modeling study of Matsuura et al. (2003) confirmed this relationship and corroborated the existence of multi-decadal TC variations in the second half of the 20th century.

The results of this study suggest that the CCLM simulations provide very valuable insights on TC climatology for the satellite era (1978–2010), including spatio-temporal TC variations and their linkage to the large-scale circulation features. They reproduce the observed interannual-to-decadal variability of TC activity as well as their upward trend. However, thorough analysis of the simulations for the whole 1948–2010 period suggests that TC activity in the pre-satellite era (e.g. intensity and frequency) is severely underestimated, compared to the latter period. This casts doubt on the physical significance of the reconstructed increase for the period 1948–2010. The analysis can't rule out an alternative hypothesis, namely that TCs predominantly experience strong multi-decadal variations. The quantification of the relative importance of these two components of variability as well as their origin is an issue requiring further investigation. Finally, we recommend that caution should be used when interpreting long-term TC statistics, either when using atmospheric reanalyses or BTD sets in the pre-satellite period.

Acknowledgements The authors are grateful to Tom Knutson, Ming Zhao and Hans von Storch for helpful comments and discussion. The work was partly supported through the Cluster of Excellence 'CliSAP' (EXC177), University of Hamburg, funded through the German Research Foundation (DFG), through the Helmholtz-Zentrum Geesthacht, Centre for Materials and Coastal Research. WZ was partially supported by the National Natural Science Foundation of China (41575078). The authors would like to thank colleagues who provided best track data sets from the Japan Meteorological Agency. The German Climate Computing Center (DKRZ) provided the computer hardware for the LAM simulations in the Regional Atmospheric Modeling project. The NCEP/NCAR reanalysis data were provided by the NCAR. The authors are grateful to ECMWF for providing ERA-40 as boundary conditions for their regional climate model. This work is a contribution to the "Helmholtz Climate Initiative REKLIM"

(Regional Climate Change), a joint research project of the Helmholtz Association of German research centres (HGF).

Open Access This article is distributed under the terms of the Creative Commons Attribution 4.0 International License (<http://creativecommons.org/licenses/by/4.0/>), which permits unrestricted use, distribution, and reproduction in any medium, provided you give appropriate credit to the original author(s) and the source, provide a link to the Creative Commons license, and indicate if changes were made.

References

- Allen MR, Robertson AW (1996) Distinguishing modulated oscillations from coloured noise in multivariate datasets. *Clim Dyn* 12:775–784
- Allen MR, Smith LA (1996) Monte Carlo SSA: detecting irregular oscillations in the presence of coloured noise. *J Clim* 9:3373–3404
- Au-Yeung AYM, Chan JCL (2012) Potential use of a regional climate model in seasonal tropical cyclone activity predictions in the western North Pacific. *Clim Dyn* 39:783–794
- Barcikowska M, Feser F, von Storch H (2012) Usability of best track data in climate statistics in the western North Pacific. *Mon Weather Rev* 140:2818–2830
- Bassist AN, Chelliah M (1997) Comparison of tropospheric temperatures derived from the NCEP/NCAR reanalysis, NCEP operational analysis, and the Microwave Sounding Unit. *Bull Amer Meteor Soc* 78:1431–1447
- Bengtsson L, Hodges KI, Esch M, Keenlyside N, Kornblueh L, Luo J-J, Yamagata T (2007) How may tropical cyclones change in a warmer climate? *Tellus A* 59(4):539–561
- Böhm U, Kücken M, Ahrens W, Block A, Hauffe D, Keuler K, Rockel B, Will A (2006) CLM—the climate version of LM: brief description and long-term applications. *COSMO Newsl* 6:225–235
- Brassington GB (1997) The modal evolution of the southern oscillation. *J Clim* 10(5):1021–1034
- Broomhead DS, King GP (1986) Extracting qualitative dynamics from experimental data. *Phys D* 20:217–236
- Camargo SJ, Barnston AG (2009) Experimental dynamical seasonal forecasts of Tropical Cyclone activity at IRI. *Weather Forecast* 24(2):472–491
- Camargo SJ, Robertson AW, Gaffney SJ, Smyth P, Ghil M (2007) Cluster analysis of typhoon tracks. Part II: large-scale circulation and ENSO. *J Clim* 20(14):3654–3676
- Camargo S, Sobel A (2005) Western North Pacific tropical cyclone intensity and ENSO. *J Clim* 18:2996–3006
- Cha D-H, Jin C-S, Lee D-K, Kuo Y-H (2011) Impact of intermittent spectral nudging on regional climate simulation using Weather Research and Forecasting model. *J Geophys Res* 116:D10103
- Chan JCL (2000) Tropical cyclone activity over the western North Pacific associated with El Niño and La Niña events. *J Clim* 13(16):2960–2972. doi:10.1175/1520-0442(2000)013<2960:TCAOTW>2.0.CO;2
- Chun-Chieh W, Zhan R, Yi L, Wang Y (2012) Internal variability of the dynamically downscaled tropical cyclone activity over the western North Pacific by the IPRC regional atmospheric model. *J Clim* 25:2104–2122
- Compo GP, Whitaker JS, Sardeshmukh PD, Matsui N, Allan RJ, Yin X, Gleason BE, Vose RS, Rutledge G, Bessemoulin P, Brönnimann S, Brunet M, Crouthamel RI, Grant AN, Groisman PY, Jones PD, Kruk MC, Kruger AC, Marshall GJ, Maugeri M, Mok HY, Nordli Ø, Ross TF, Trigo RM, Wang XL, Woodruff SD, Worley SJ (2011) The twentieth century reanalysis project. *Q J R Meteorol Soc* 137(654):1–28
- Deser C, Phillips AS, Hurrell JW (2004) Pacific interdecadal climate variability: linkages between the tropics and North Pacific during boreal winter since 1900. *J Clim* 17:3109–3124
- Emanuel KA (2005) Increasing destructiveness of tropical cyclones over the past 30 years. *Nature* 436:686–688
- Emanuel KA (2007) Environmental factors affecting tropical cyclone power dissipation. *J Clim* 20:5497–5509
- Emanuel K, Sundararajan R, Williams J (2008) Hurricanes and global warming: results from downscaling IPCC AR4 simulations. *Bull Am Meteorol Soc* 89(3):347–367
- Feser F, Barcikowska M (2012) The influence of spectral nudging on typhoon formation in regional climate models. *Environ Res Lett* 7(014):024
- Feser F, von Storch H (2005) A spatial two-dimensional discrete filter for limited area model evaluation purposes. *Mon Weather Rev* 133(6):1774–1786
- Feser F, von Storch H (2008a) Regional modelling of the western Pacific typhoon season 2004. *Meteorol Z* 17(4):519–528
- Feser F, von Storch H (2008b) A dynamical downscaling case study for Typhoons in Southeast Asia using a regional climate model. *Month Weather Rev* 136:1806–1815. doi:10.1175/2007MWR2207.1
- Fraedrich K (1986) Estimating the dimensions of weather and climate attractors. *J Atmos Sci* 43:419–432
- Huang W-R, Chan JL (2014) Dynamical downscaling forecasts of western North Pacific tropical cyclone genesis and landfall. *Clim Dyn* 42(7–8):2227–2237
- Iizuka S, Matsuura T (2008) ENSO and Western North Pacific tropical cyclone activity simulated in a CGCM. *Clim Dyn* 30(7–8):815–830
- Kalnay E et al (1996) The NCEP/NCAR 40-year reanalysis project. *Bull Am Meteorol Soc* 77:437–470
- Kamahori H, Yamazaki N, Mannoji N, Takahashi K (2006) Variability in intense tropical cyclone days in the western North Pacific. *SOLA* 2:104–107
- Kamahori H et al (2011) Future changes in tropical cyclone activity projected by the new high-resolution MRI-AGCM. *J Clim* 25(9):3237–3260
- Kaplan A, Cane M, Kushnir Y, Clement AC, Blumenthal M, Rajagopalan B (1998) Analyses of global sea surface temperature 1856–1991. *J Geophys Res* 103:18567–18589. doi:10.1029/97JC01736
- Kaplan A, Kushnir Y, Cane M (2000) Reduced space optimal interpolation of historical marine sea level pressure: 1854–1992. *J Clim* 13:2987–3002
- Kim H-M, Webster PJ, Curry JA (2010) Modulation of North Pacific tropical cyclone activity by three phases of ENSO. *J Clim* 24(6):1839–1849
- Knutson TR, Sirutis JJ, Garner ST, Held IM, Tuleya RE (2007) Simulation of the recent multidecadal increase of Atlantic hurricane activity using an 18-km-grid regional model. *Bull Am Meteorol Soc* 88(10):1549–1565
- Krueger O, Schenk F, Feser F, Weisse R (2013) Inconsistencies between Long-Term Trends in storminess derived from the 20CR reanalysis and observations. *J Clim* 26(3):868–874
- Knutson TR, Tuleya RE, Kurihara Y (1998) Simulated increase of hurricane intensities in a CO₂-warmed climate. *Science* 279(5353):1018–1021. doi:10.1126/science.279.5353.1018
- Landsea CW (1993) A climatology of intense (or major) atlantic hurricanes. *Mon Weather Rev* 121:1703–1713
- Landsea C, Harper B, Hoarau K, Knaff JA (2006) Can we detect trends in extreme tropical cyclones? *Science* 313:452–454
- Liu K, Chan J (2008) Interdecadal variability of western North Pacific tropical cyclone tracks. *J Clim* 21:4464–4476

- Liu K, Chan J (2013) Inactive period of western North Pacific tropical cyclone activity in 1998–2011. *J Clim* 26(8):2614–2630
- Luo J-J, Yamagata T (2001) Long-term El Niño-southern oscillation (ENSO)-like variation with special emphasis on the south Pacific. *J Geophys Res* 106(22):211–227
- Matsuura T, Yumoto M, Iizuka S (2003) A mechanism of interdecadal variability of tropical cyclone activity over the western North Pacific. *Clim Dyn* 21(2):105–117
- Meehl GA, Aixue Hu, Arblaster JM, Fasullo J, Trenberth KE (2013) Externally forced and internally generated decadal climate variability associated with the interdecadal Pacific oscillation. *J Clim* 26:7298–7310. doi:[10.1175/JCLI-D-12-00548.1](https://doi.org/10.1175/JCLI-D-12-00548.1)
- Mei W, Shang-Ping X, Zhao M, Wang Y (2015) Forced and internal variability of tropical cyclone track density in the western North Pacific. *J Clim* 28(1):143–167. doi:[10.1175/JCLI-D-14-00164.1](https://doi.org/10.1175/JCLI-D-14-00164.1)
- Murakami H, Mizuta R, Shindo E (2012) Future changes in tropical cyclone activity projected by multi-physics and multi-sst ensemble experiments using the 60-km-mesh MRI-AGCM. *Clim Dyn* 39(9–10):2569–2584
- Newman M, Alexander MA, Ault TR, Cobb KM, Deser C, Di Lorenzo E, Mantua NJ, Miller AJ, Minobe S, Nakamura H, Schneider N, Vimont DJ, Phillips AS, Scott JD, Smith CA (2016) The Pacific decadal oscillation, revisited. *J Clim* 29:4399–4427. doi:[10.1175/JCLI-D-15-0508.1](https://doi.org/10.1175/JCLI-D-15-0508.1)
- Oouchi K, Yoshimura J, Yoshimura H, Mizuta R, Kusunoki S, Noda A (2006) Tropical cyclone climatology in a global-warming climate as simulated in a 20 km-mesh global atmospheric model: frequency and wind intensity analyses. *J Meteor Soc Japan* 84(2):259–276
- Power S et al (1999) Interdecadal modulation of the impact of ENSO on Australia. *Clim Dyn* 15:319–324
- Ren F, Liang J, Wu G, Dong W, Yang X (2011) Reliability analysis of climate change of tropical cyclone activity over the western North Pacific. *J Clim* 24(22):5887–5898
- Rockel B, Will A, Hense A (2008) The regional climate model COSMO-CLM (CCLM). *Meteorol Z* 12:347–348
- Song J-J, Wang Y, Wu L (2010) Trend discrepancies among three best track data sets of western North Pacific tropical cyclones. *J Geophys Res* 115:D12128. doi:[10.1029/2009JD013058](https://doi.org/10.1029/2009JD013058)
- Steppeler J, Doms G, Schaettler U, Bitzer H-W, Gassmann A, Darrath U, Gregoric G (2003) Meso-gamma scale forecasts using the nonhydrostatic model LM. *Meteorol Atmos Phys* 82:75–96. doi:[10.1007/s00703-001-0592-9](https://doi.org/10.1007/s00703-001-0592-9)
- Stowasser M, Wang Y, Hamilton K (2007) Tropical cyclone changes in the western North Pacific in a global warming scenario. *J Clim* 20(11):2378–2396
- Sturaro G (2003) A closer look at the climatological discontinuities present in the NCEP/NCAR reanalysis temperature due to the introduction of satellite data. *Clim Dyn* 21(3–4):309–316
- Sugi M, Yoshimura J (2004) A mechanism of tropical precipitation change due to CO₂ increase. *J Clim* 17(1):238–243
- Sugi M, Yoshimura J (2012) Decreasing trend of tropical cyclone frequency in 228-year high-resolution AGCM simulations. *Geophys Res Lett* 39(19):L19805. doi:[10.1029/2012GL053360](https://doi.org/10.1029/2012GL053360)
- Sugi M, Noda A, Sato N (2002) Influence of the global warming on tropical cyclone climatology: an experiment with the JMA global model. *J Meteor Soc Japan* 80(2):249–272
- Tiedtke M (1989) A comprehensive mass flux scheme for cumulus parameterization in large-scale models. *Mon Weather Rev* 117(8):1779–1800
- Trenberth KE, Stepaniak DP, Hurrell JW, Fiorino M (2001) Quality of reanalyses in the tropics. *J Clim* 14(7):1499–1510
- Tourre YM, Rajagopalan B, Kushnir Y, Barlow M, Warren B (2001) Patterns of coherent decadal and interdecadal climate signals in the Pacific basin during the 20th century. *Geophys Res Lett* 28:2069–2072. doi:[10.1029/2000GL012780](https://doi.org/10.1029/2000GL012780)
- Uppala SM et al (2005) The ERA-40 re-analysis. *Q J R Meteorol Soc* 131(612):2961–3012
- Vecchi GA, Fueglistaler S, Held IM, Knutson TR, Zhao M (2013) Impacts of atmospheric temperature trends on tropical cyclone activity. *J Clim* 26(11):3877–3891
- Velden C et al (2006) The dvorak tropical cyclone intensity estimation technique: a satellite-based method that has endured for over 30 years. *Bull Am Meteorol Soc* 87(9):S6–S9
- Vitart F, Anderson JL, Stern WF (1997) Simulation of interannual variability of tropical storm frequency in an ensemble of GCM integrations. *J Clim* 10(4):745–760
- von Storch H, Langenberg H, Feser F (2000) A spectral nudging technique for dynamical downscaling purposes. *Mon Weather Rev* 128(10):3664–3673
- Walsh KJE, Nguyen K-C, McGregor JL (2004) Fine-resolution regional climate model simulations of the impact of climate change on tropical cyclones near Australia. *Clim Dyn* 22:47–56
- Wang B, Chan JCL (2002) How strong ENSO events affect tropical storm activity over the western North Pacific. *J Clim* 15:1643–1658
- White WB, Tourre Y (2003) Global SST/SLP waves during the 20th century. *Geophys Res Lett* 30(12):1651. doi:[10.1029/2003GL017055](https://doi.org/10.1029/2003GL017055)
- White WB, Tourre Y, Barlow M, Dettinger M (2003) A delayed action oscillator shared by biennial, interannual, and decadal signals in the Pacific basin. *J Geophys Res* 108(c3):3070. doi:[10.1029/2002JC001490](https://doi.org/10.1029/2002JC001490)
- Wu M-C, Yeung K-H, Chang W-L (2006) Trends in western North Pacific tropical cyclone intensity. *Eos Trans AGU* 87(48):537–538
- Wu L, Wen Z, Huang R, Wu R (2012) Possible linkage between the monsoon trough variability and the tropical cyclone activity over the western North Pacific. *Mon Weather Rev* 140(1):140–150
- Wu L et al (2014) Simulations of the present and late-twenty-first-century western North Pacific tropical cyclone activity using a regional model. *J Clim* 27:3405–3424
- Xie SP (1996) Westward propagation of latitudinal asymmetry in a coupled ocean-atmosphere model. *J Atmos Sci* 53:3236–3250
- Xie SP, Philander SGH (1994) A coupled ocean-atmosphere model of relevance to the ITCZ in the eastern Pacific. *Tellus Ser A* 46:340–350
- Zhang W, Vecchi GA, Murakami H, Delworth T, Wittenberg AT, Rosati A, Underwood S, Anderson W, Harris L, Gudgel R, Lin SJ, Villarini G, Chen JH (2016) Improved simulation of tropical cyclone responses to ENSO in the western North Pacific in the high-resolution GFDL HiFLOR coupled climate model. *J Clim* 29:1391–1415
- Zhao M, Held IM, Lin S-J, Vecchi GA (2007) Simulations of global hurricane climatology, interannual variability, and response to global warming using a 50-km resolution GCM. *J Clim* 22:6653–6678. doi:[10.1175/2009JCLI3049](https://doi.org/10.1175/2009JCLI3049)